2. ANALYTIC METHODS

2.1 Whole-rock Major and Trace Elements and Sr-Nd Isotope

Total of seventeen samples (including three aplites) show no or least altered rocks have been analyzed for whole-rock major and trace elements. Among them, whole-rock Sr and Nd isotopic compositions were measured for 2 aplites and 6 granodiorites. *In-situ* zircon U-Pb and O isotopic compositions were determined for one granodiorite and an aplite sample by secondary ion mass spectrometry. All of these analyses were carried out at the State Key Laboratory of Isotope Geochemistry, Guangzhou Institute of Geochemistry, Chinese Academy of Sciences.

A Rigaku RIX 2000 X-ray fluorescence spectrometer was used for whole-rock major element oxides determination. Detailed analytic procedure and equipment run conditions are described as Li et al. (2004). Calibration lines produced by bivariate regression of measurements of 36 references materials encompassing a wide range of silicate compositions were used for data quantification. Analytical variations are between 1 wt.% and 5 wt.%.

Each powdered sample was dissolved in a high-pressure Teflon bomb for over 48 hours with a HF + HNO_3 mixture for trace element concentrations analyses. An Agilent 7500a ICP-MS was utilized for trace elements detection. Analytical presision typically is better than 3%. During analytical procedure, the signal drift during peak counting was monitored with addition of an internal standard solution containing the single element Rh (Li et al., 2004).

Whole-rock radiogenic Sr-Nd isotopic compositions were determined with a Nu

instruments Plasma MC-ICP-MS, the analytical procedures were similar to those detailed by Li et al. (2006). Chemical separation and purification of Nd were conducted through conventional cation columns followed by HDEHP columns. The Sr was separated using cation exchange, and purified in a Teflon column using Eichrom Sr Spec resin. Sr and Nd isotopic compositions were normalized for mass fractionation relative to $^{146}Nd/^{144}Nd = 0.7219$ and $^{86}Sr/^{88}Sr = 0.1194$. All Nd duplicate analyses agree within the analytical errors defined by replicate analyses of the Shin Etsu JNdi-1 Nd standard. During the analysis session for our samples, the average $^{143}Nd/^{144}Nd$ value of 5 analyses of the Shin Etsu JNdi-1 Nd standard is 0.512114 ± 0.000005, the measured value of BCR-2 and JB-3 is 0.512621 (recommended value = 0.512637 ± 0.000012) and 0.513054 ± 0.000004, respectively. The measured mean value of 5 analyses of NBS987 Sr standard is $^{87}Sr/^{86}Sr$=0.710259 ± 0.000008, the measured value of BHVO-2 and JB-3 standard is 0.703482 (recommended value = 0.703479 ± 0.000020) and 0.703444, respectively.

2.2 Zircon U-Pb and O Isotope

Zircons were separated and concentrated from approximately 2 kg of each sample by conventional magnetic and density techniques. Zircon crystals, together with zircon standards Qinghu, Plešovice, and Penglai were mounted in epoxy resin mounts. Zircons were selected following transmitted and reflected light photomicrographs, as well as cathodoluminescence (CL) imaging.

Zircon U-Th-Pb ratios were determined relative to the standard zircon Plešovice,

and the absolute abundances were calibrated to the standard zircon Penglai, operating and data processing procedures are similar to those outlined by Li et al. (2009). The weighted mean U-Pb ages and Concordia plots were processes using Isoplot/Ex v.3.0 program (Ludwig, 2003). Detailed analytical data are given in Supplementary Data Table 1, and Concordia plots are presented in Figure DR2, in which individual spots are show at 1σ uncertainties, whereas the weighted mean ages are quoted at 2σ uncertainties level. The detailed procedures for zircon O isotope were similar to those described by Li et al. (2013). The measured O isotopic data were corrected for instrumental mass fractionation using the Penglai zircon standard. During the course of this study, ten measurements of the zircon standard Penglai yielded a weighted mean of $\delta^{18}O = 5.25 \pm 0.20$ permil, five analyses of the zircon Qinghu provided mean value of 5.53 ± 0.18 permil (Li et al., 2013).

3. RESULTS

3.1 Zircon SIMS U-Pb Dating Results

Granodiorite sample 16KQ02-2 represents the main body of the Kangqiong pluton was dated (Figure DR2). Twenty spots on 16 zircon crystals yielded apparent $^{206}Pb/^{238}U$ age ranging from 141.7 to 158.2 Ma. Among them, one spot given a apparent $^{206}Pb/^{238}U$ age of 151.3 Ma that have low measured $^{206}Pb/^{204}Pb$ ratio (972) indicates high common Pb concentration, another two spots yielded discernable younger age (~143 Ma) than remaining spots. Then, the remaining 17 analyses yielded a weighted mean age of 154.6 ± 1.6 Ma (MSWD = 0.42, n = 17), and a

concordia age of 154.4 ± 0.8 (MSWD = 2.4).

Fifteen spot were carried out on 15 zircon grains from aplite sample (16KQ01-3). One spot yielded a significant old age of 227.3 Ma, which possibly represent captured or inherited zircon. The remaining measured zircon provided apparent age ranging from 142.5 to 158.9 Ma. Two spots possibly result from later crystallization or weakly loss of radiogenic Pb, they yielded age of ~143 Ma. The remaining 12 spots yielded weighted mean age of 153.1 ± 2.6 Ma (MSWD = 1.4), and provided a concordia age of 153.0 ± 1.0 Ma (MSWD = 2.1).

3.2 Major and Trace Element Geochemical Composition

Granodiorite of the Kangqiong pluton have homogeneous and intermediate SiO_2 contents (64.2 to 68.2 wt.%, mean of 65.6 wt.%), high in Al_2O_3 (>15.2 wt.%). They are Na_2O-rich (4.59 7.07 wt.%) and have K_2O/Na_2O ratio < 0.5. All of them are metaluminous with A/CNK ($Al_2O_3/[CaO + Na_2O + K_2O]$ in molar) values < 1. These rocks have high MgO (1.48 to 3.22, mean of 2.63 wt.%) with Mg# between 41 and 69 (Mean of 62). Aplite samples have higher SiO_2 (>72 wt.%), K_2O (> 4.0 %), but lower MgO and others major element contents than those of the granodiorites.

The granodiorites in the Kangqiong area have variable Cr (from 60.9 to 117 ppm) and Ni (27.2 to 55.1 ppm) contents. They are characterized by their high Sr content (460 to 1097 ppm), and low Yb (< 1.26 ppm) and Y (< 13.3 ppm). Therefore, these granodiorite have high Sr/Y ratios (> 40) and La/Yb ratios (5.82 to 24.7). In addition, they exhibit high Nb/Ta (11.9 to 14.5), Zr/Hf (38 to 41), and Th/La (0.30 to 0.62). The

granodiorite show weakly negative or no anomalies in Eu (Eu/Eu* = 0.85 ~ 1.11) on chondrite-normalized REE pattern plots, and fractionated REE patterns with $(La/Yb)_N$ = 5.8 ~ 17.7. On the contrary, aplites show similar REE pattern with granodiorite but with significant depletion in Eu (0.51 ~ 0.62) and relatively low in MREE elements. The evolved features of aplite are evident as indicated by their high Rb, Th, and strong trough in P, Ti and Ba.

3.3 Whole-Rock Sr-Nd and Zircon Stable O Isotopic Composition

Analyzed granodiorite have relatively high initial $^{87}Sr/^{86}Sr$ ratios ranging from 0.70501 to 0.70718, the initial $^{143}Nd/^{144}Nd$ ratios between 0.512399 and 0.512539 and calculated εNd (t = 156 Ma) range from -0.79 to +1.95. Two analyses of aplite have initial $^{87}Sr/^{86}Sr$ ratios in the range from 0.70618 to 0.70640, and εNd (t = 156 Ma) values of -0.50 and -1.40.

Twenty-nine O isotope analyses were conducted on 22 zircon crystals from granodiorite unit. Two measurements on zircon inner and rim were obtained for 8 large zircon individuals. When zircon inner and rim pairs analyzed for single zircon crystal, the inner portion typically show heavier $\delta^{18}O$ value than their rim, rare of this difference is >1 ‰. One rim yielded a low $\delta^{18}O$ value of 3.63‰, this is unreliable since the ablated zircon domain was cracked. One paired inner-rim spots revealed a lighter $\delta^{18}O$ value for inner part than their rim, this rim have high common Pb concentration. Among them, the 8 inner spots from paired inner-rim suites yielded a mean $\delta^{18}O$ value of 5.56 ‰, 6 spots on rim given mean values of 5.23‰. Excluding

the two outliers, remaining 28 spots show variable $\delta^{18}O$ value varying from 4.61 to 6.17 ‰ with mean of 5.6 ± 0.36‰. Zircons from aplite sample revealed stable zircon $\delta^{18}O$ value ranging from 4.04 to 7.65 ‰ with mean of 5.52 ± 0.64‰; with one exception have significantly low $\delta^{18}O$ value of 1.83‰ that may result from zircon remobilization or radiogenic damage as indicated by the small muddy spot on zircon CL image.

Cited References:

Li, X.-H., Li, Z.-X., Wingate, M. T. D., Chung, S.-L., Liu, Y., Lin, G.-C., and Li, W.-X., 2006, Geochemistry of the 755 Ma Mundine Well dyke swarm, northwestern Australia: Part of a Neoproterozoic mantle superplume beneath Rodinia?: Precambrian Research, v. 146, no. 1, p. 1-15.

Li, X.-H., Liu, D.-Y., Sun, M., Li, W.-X., Liang, X.-R., and Liu, Y., 2004, Precise Sm-Nd and U-Pb isotopic dating of the supergiant Shizhuyuan polymetallic deposit and its host granite, SE China: Geological Magazine, v. 141, no. 2, p. 225-231.

Li, X.-H., Liu, Y., Li, Q.-L., Guo, C.-H., and Chamberlain, K. R., 2009, Precise determination of Phanerozoic zircon Pb/Pb age by multicollector SIMS without external standardization: Geochemistry, Geophysics, Geosystems, v. 10, no. 4, p. Q04010.

Li, X. H., Tang, G. Q., Gong, B., Yang, Y. H., Hou, K. J., Hu, Z. C., Li, Q. L., Liu, Y., and Li, W. X., 2013, Qinghu zircon: A working reference for microbeam analysis of U-Pb age and Hf and O isotopes: Science Bulletin, v. 58, no. 36, p. 4647-4654.

Ludwig, K. R., 2003, User's manual for Isoplot 3.0: A geochronological toolkit for

134 microsoft excel: Berkeley Geochronology Center, Berkeley Geochronology Center.

Fig. DR1

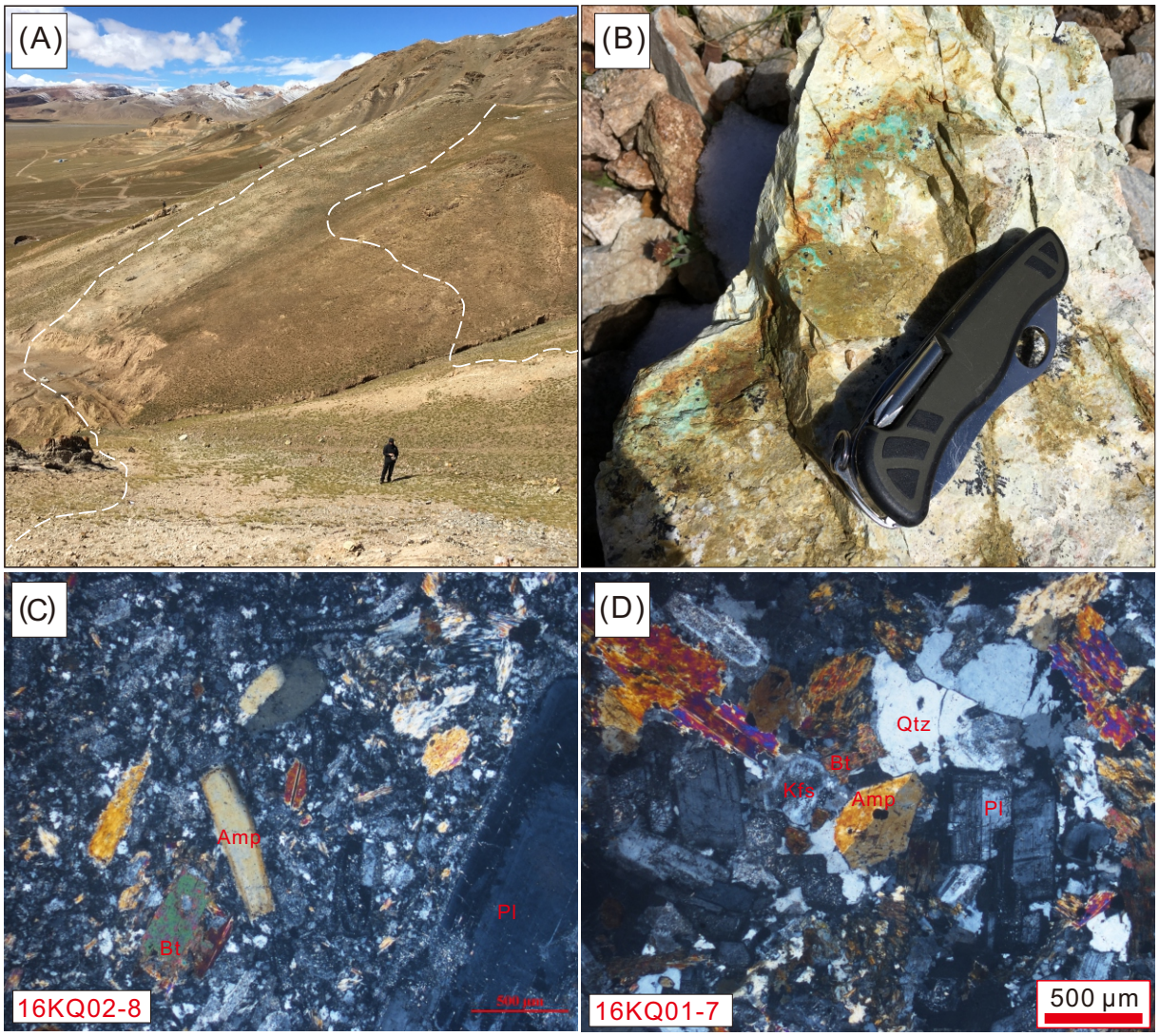

By Yang, Wang, Hao and coauthors
for MS 48486R adakites in central Tibet

Fig. DR1. Representative field photographs (A, B) and thin-section photographs (C, D; cross polarized) for the Kangqiong (KQ) plutons. The white dashed lines in (A) show the contacts with Jurassic sedimentary rocks; (B) copper mineralization of the intrusion; (C, D) show porphyritic and equigranular texture of the KQ plutons, respectively. Abbreviation: Amp, amphibole; Bt, biotite; Kfs, K-feldspar; Pl, plagioclase; Qtz: quartz.

Fig. DR2

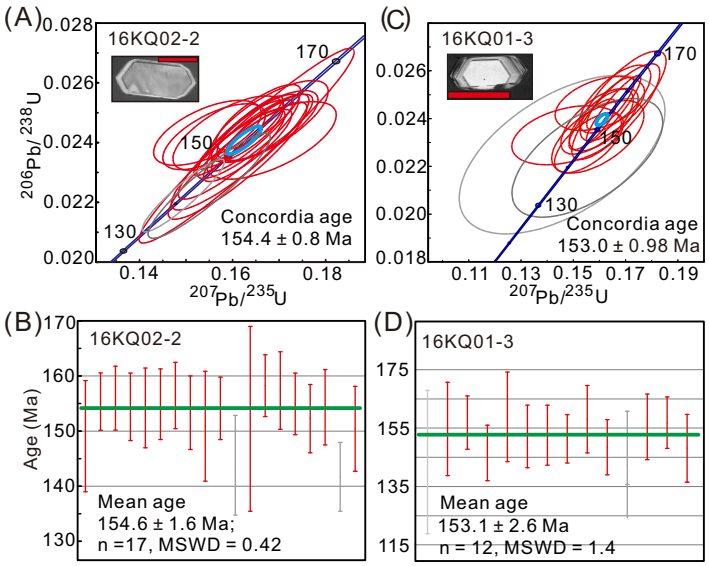

By Yang, Wang, Hao and coauthors
for MS 48486R adakites in central Tibet

Fig. DR2. SIMS zircon U-Pb ages and representative Cathodoluminescence (CL) images for the KQ plutons. Gray circles (A, C) and (B, D) bars are data points excluded from Concordia and weighted mean age calculations.

Fig. DR3

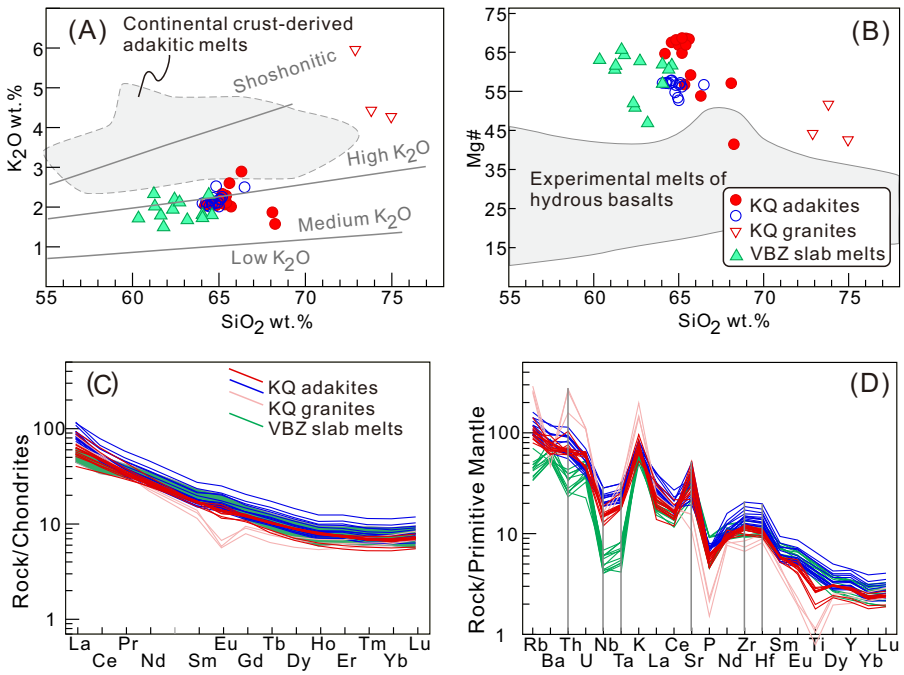

By Yang, Wang, Hao and coauthors

for MS 48486R adakites in central Tibet

Fig. DR3. (A, B) K_2O and Mg# versus SiO2, respectively; (C) Chondrite-normalized rare earth elements patterns; (D) Primitive mantle-normalized trace-elements distribution patterns of the KQ plutons. The continental crust-derived adakitic melts are after (Wang et al., 2008); The Valle de Bravo-Zitácuaro (VBZ) slab melts (late Cenozoic volcanic rocks from central Mexico) are from Gómez-Tuena et al. (2007); The experimental melts of natural hydrous basalts produced at 1-4 GPa are from Sen and Dunn (1994), Rapp (1995), Rapp et al. (1999), Rapp and Watson (1995). The values of the chondrite and primitive mantle are from Sun and McDonough (1989). Filled red (this study) and open blue cycles (Li et al., 2016) are KQAs, and the reverse triangles are fine-grained granites of the KQ plutons. Cited data are the same in following, except where specified.

Fig. DR4

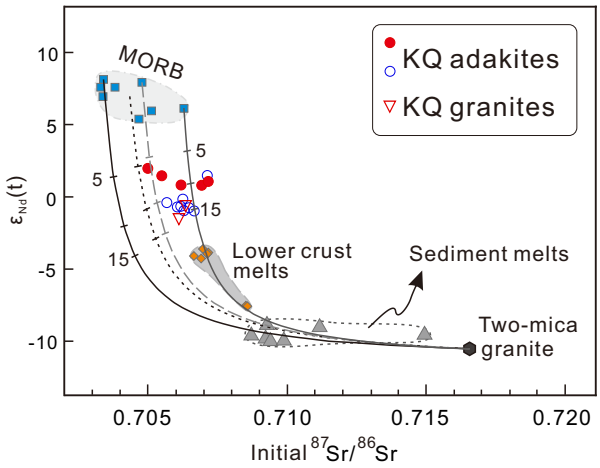

By Yang, Wang, Hao and coauthors

for MS 48486R adakites in central Tibet

Fig. DR4. Whole-rock Sr-Nd isotope plot. The field of sediment melts is defined by ~162 Ma high-Mg andesites in western Amdo area, SQT (Zeng et al., 2016); the lower crust melts denote ~152 Ma adakitic granodiorites from the Gerze area, SQT (Hao et al., 2019, and references therein); the two-mica granites are representative of the basement component of SQT (Hu et al., 2015); the middle oceanic ridge basalts (MORBs) are from Wang et al. (2016).

Fig. DR5

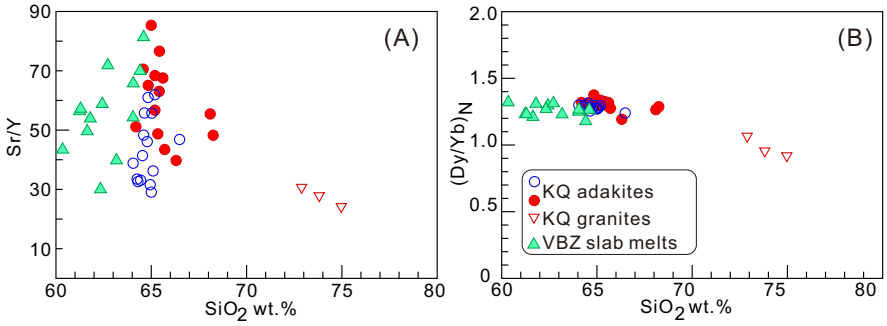

By Yang, Wang, Hao and coauthors
for MS 48486R adakites in central Tibet

Fig. DR5. (A) whole-rock Sr/Y and (B) chondrite-normalized Dy/Yb versus SiO_2 for the KQ plutons. The Sr/Y and (Dy/Yb)N ratios show no positive correlation with SiO_2 contents, indicating garnet fractionation is negligible. Weak fractional crystallization of amphibole is possible for the KQ granites, but is unsuitable for the KQAs. Values of the chondrites are from Sun and McDonough (1989).

Fig. DR6

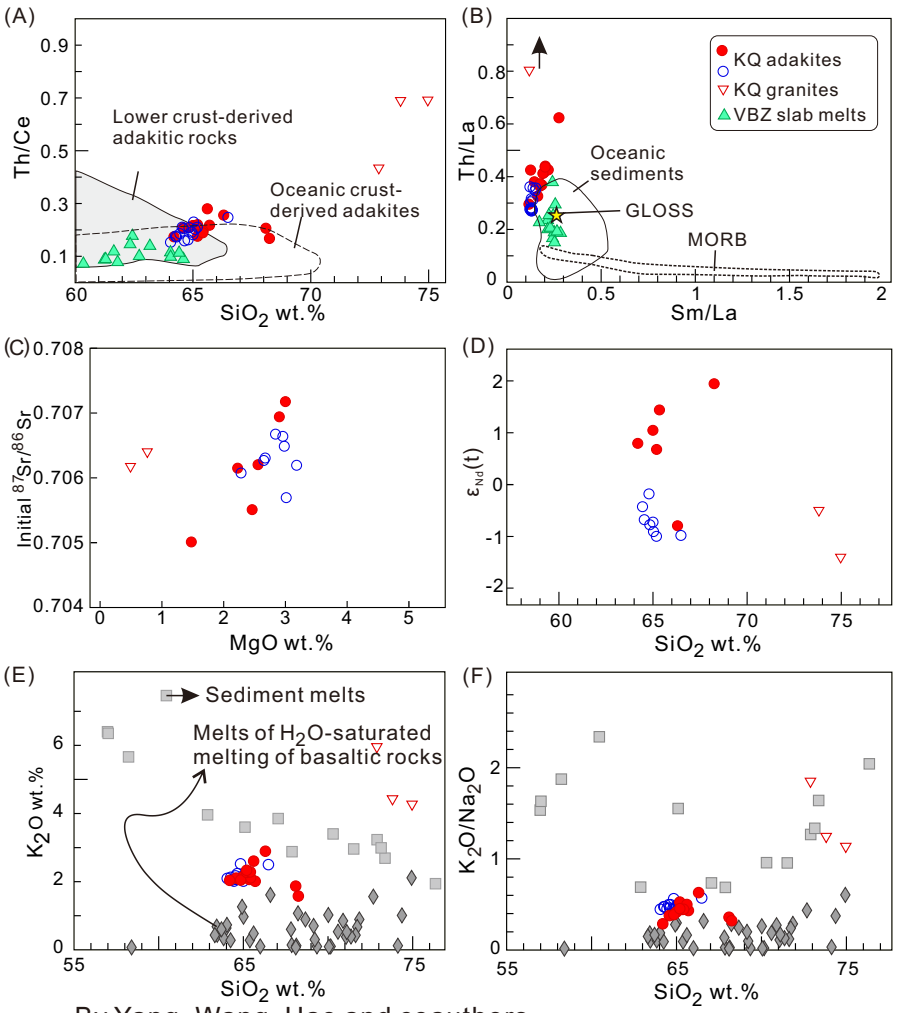

By Yang, Wang, Hao and coauthors

for MS 48486R adakites in central Tibet

Fig. DR6. (A) Th/Ce versus SiO_2 plots (after Wang et al., 2006, and references therein); (B) Th/La versus Sm/La plot, after the concept of Plank (2005). The higher Th/La ratios of the KQAs than those of MORBs indicate the contribution of continental components. (C) Initial Sr isotopes versus MgO; (D) Calculated εNd(t = 154 Ma) values versus SiO_2 contents. Slightly positive correlation between initial $^{87}Sr/^{86}Sr$ and MgO and no obvious correlation between εNd(t) and SiO2 inconsistent with crustal contamination or the delaminated lower crustal melting model Wang et al. (2006, 2008). (E, F) K_2O and K_2O/Na_2O versus SiO_2 for the KQ plutons, repectively. Sediment melts have higher K_2O and K_2O/Na_2O than the KQAs, indicating that partial melting of sediments is not suitable for the KQAs. The sediments melts are from Johnson and Plank (2000) and melts of water-saturated melting of basaltic rocks are from Beard and Lofgren (1991).

Fig. DR7

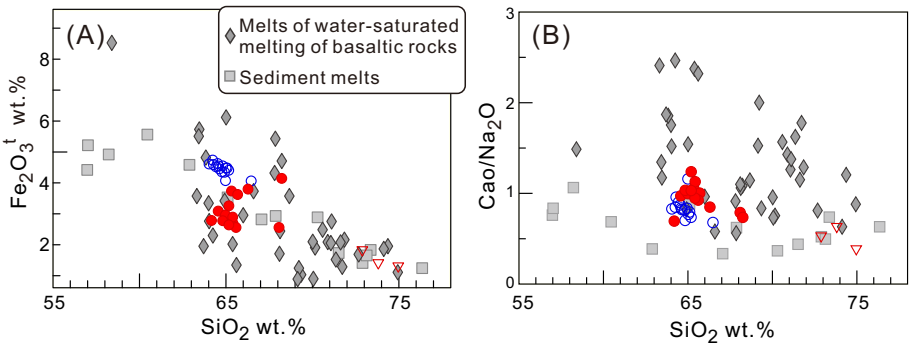

By Yang, Wang, Hao and coauthors
for MS 48486R adakites in central Tibet

Fig. DR7. (A, B) $Fe_2O_3^t$ and CaO/Na_2O versus SiO_2, respectively. The KQAs have $Fe_2O_3^t$ contents and CaO/Na_2O ratios comparable with experimental melts of water saturated basaltic rocks, which indicate that the parental magmas of the KQAs were formed by water-fluxed melting.

Fig. DR8

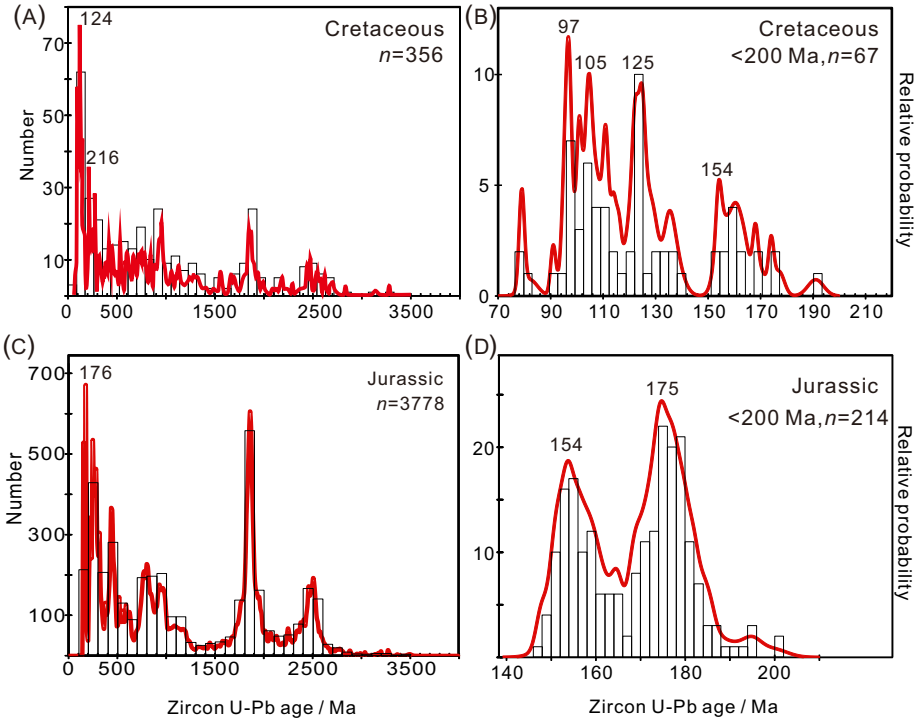

By Yang, Wang, Hao and coauthors
for MS 48486R adakites in central Tibet

Fig. DR8. Detrital zircon U-Pb ages of Jurassic (C, D) and Cretaceous sedimentary rocks (A, B) in SQT, the right columns (B, D) are plots of the zircons age < 200 Ma. The data are from Huang et al. (2017), Li et al. (2017a, b) and Ma et al. (2017).

REFERENCES CITED

Beard, J. S., and Lofgren, G. E., 1991, Dehydration Melting and Water-Saturated Melting of Basaltic and Andesitic Greenstones and Amphibolites at 1, 3, and 6. 9 kb: Journal of Petrology, v. 32, no. 2, p. 465-501.

Gómez-Tuena, A., Langmuir, C. H., Goldstein, S. L., Straub, S. M., and Ortega-Gutiérrez, F., 2007, Geochemical Evidence for Slab Melting in the Trans-Mexican Volcanic Belt: Journal of Petrology, v. 48, no. 3, p. 537-562.

Hu, P.-Y., Zhai, Q.-G., Jahn, B.-M., Wang, J., Li, C., Lee, H.-Y., and Tang, S.-H., 2015, Early Ordovician granites from the South Qiangtang terrane, northern Tibet: Implications for the early Paleozoic tectonic evolution along the Gondwanan proto-Tethyan margin: Lithos, v. 220–223, p. 318-338.

Huang, T.-T., Xu, J.-F., Chen, J.-L., Wu, J.-b., and Zeng, Y.-C., 2017, Sedimentary record of Jurassic northward subduction of the Bangong–Nujiang Ocean: insights from detrital zircons: International Geology Review, v. 59, no. 2, p. 166-184.

Johnson, M. C., and Plank, T., 2000, Dehydration and melting experiments constrain the fate of subducted sediments: Geochemistry, Geophysics, Geosystems, v. 1, no. 12.

Li, S., Ding, L., Guilmette, C., Fu, J., Xu, Q., Yue, Y., and Henrique-Pinto, R., 2017a, The subduction-accretion history of the Bangong-Nujiang Ocean: Constraints from provenance and geochronology of the Mesozoic strata near Gaize, central Tibet: Tectonophysics, v. 702, p. 42-60.

Li, S., Guilmette, C., Ding, L., Xu, Q., Fu, J.-J., and Yue, Y.-H., 2017b, Provenance of Mesozoic clastic rocks within the Bangong-Nujiang suture zone, central Tibet: Implications for the age of the initial Lhasa-Qiangtang collision: Journal of Asian Earth Sciences, v. 147, p. 469-484.

Li, Y., He, J., Han, Z., Wang, C., Ma, P., Zhou, A., Liu, S.-A., and Xu, M., 2016, Late Jurassic sodium-rich adakitic intrusive rocks in the southern Qiangtang terrane, central Tibet, and their implications for the Bangong–Nujiang Ocean subduction: Lithos, v. 245, p. 34-46.

Ma, A., Hu, X., Garzanti, E., Han, Z., and Lai, W., 2017, Sedimentary and tectonic evolution of the southern Qiangtang basin: implications for the Lhasa-Qiangtang collision timing: Mesozoic geology of central Tibet: Journal of Geophysical Research: Solid Earth, v. 122, no. 7, p. 4790-4813.

Plank, T., 2005, Constraints from thorium/lanthanum on sediment recycling at subduction zones and the evolution of the continents: Journal of Petrology, v. 46, no. 5, p. 921-944.

Rapp, R. P., 1995, Amphibole-out phase boundary in partially melted metabasalt, its control over liquid fraction and composition, and source permeability: Journal of

Geophysical Research: Solid Earth, v. 100, no. B8, p. 15601-15610.

Rapp, R. P., and Watson, E. B., 1995, Dehydration Melting of Metabasalt at 8-32 kbar: Implications for Continental Growth and Crust-Mantle Recycling: Journal of Petrology, v. 36, no. 4, p. 891-931.

Rapp, R. P., Shimizu, N., Norman, M. D., and Applegate, G. S., 1999, Reaction between slab-derived melts and peridotite in the mantle wedge: experimental constraints at 3.8 GPa: Chemical Geology, v. 160, no. 4, p. 335-356.

Sen, C., and Dunn, T., 1994, Dehydration melting of a basaltic composition amphibolite at 1.5 and 2.0 GPa: implications for the origin of adakites: Contributions to Mineralogy and Petrology, v. 117, no. 4, p. 394-409.

Sun, S. s., and McDonough, W. F., 1989, Chemical and isotopic systematics of oceanic basalts: implications for mantle composition and processes: Geological Society, London, Special Publications, v. 42, no. 1, p. 313.

Wang, B.-D., Wang, L.-Q., Chung, S.-L., Chen, J.-L., Yin, F.-G., Liu, H., Li, X.-B., and Chen, L.-K., 2016, Evolution of the Bangong–Nujiang Tethyan ocean: Insights from the geochronology and geochemistry of mafic rocks within ophiolites: Lithos, v. 245, p. 18-33.

Wang, Q., Wyman, D. A., Xu, J., Dong, Y., Vasconcelos, P. M., Pearson, N., Wan, Y., Dong, H., Li, C., Yu, Y., Zhu, T., Feng, X., Zhang, Q., Zi, F., and Chu, Z., 2008, Eocene melting of subducting continental crust and early uplifting of central Tibet: Evidence from central-western Qiangtang high-K calc-alkaline andesites, dacites and rhyolites: Earth and Planetary Science Letters, v. 272, no. 1, p. 158-171.

Wang, Q., Xu, J.-F., Jian, P., Bao, Z.-W., Zhao, Z.-H., Li, C.-F., Xiong, X.-L., and Ma, J.-L., 2006, Petrogenesis of Adakitic Porphyries in an Extensional Tectonic Setting, Dexing, South China: Implications for the Genesis of Porphyry Copper Mineralization: Journal of Petrology, v. 47, no. 1, p. 119-14.

Zeng, Y.-C., Chen, J.-L., Xu, J.-F., Wang, B.-D., and Huang, F., 2016, Sediment melting during subduction initiation: Geochronological and geochemical evidence from the Darutso high-Mg andesites within ophiolite mélange, central Tibet: Geochemistry Geophysics Geosystems, v. 17, no. 12, p. 4859-4877.